university of groningen

University Medical Center Groningen

University of Groningen

Discrete dislocation modelling of Nano- and Micro-indentation

Widjaja, Andreas

IMPORTANT NOTE: You are advised to consult the publisher's version (publisher's PDF) if you wish to cite from it. Please check the document version below.

Document Version
Publisher's PDF, also known as Version of record

Publication date:
2007

Link to publication in University of Groningen/UMCG research database

Citation for published version (APA):
Widjaja, A. (2007). *Discrete dislocation modelling of Nano- and Micro-indentation*. s.n.

Copyright
Other than for strictly personal use, it is not permitted to download or to forward/distribute the text or part of it without the consent of the author(s) and/or copyright holder(s), unless the work is under an open content license (like Creative Commons).

The publication may also be distributed here under the terms of Article 25fa of the Dutch Copyright Act, indicated by the "Taverne" license. More information can be found on the University of Groningen website: https://www.rug.nl/library/open-access/self-archiving-pure/taverne-amendment.

Take-down policy
If you believe that this document breaches copyright please contact us providing details, and we will remove access to the work immediately and investigate your claim.

Downloaded from the University of Groningen/UMCG research database (Pure): http://www.rug.nl/research/portal. For technical reasons the number of authors shown on this cover page is limited to 10 maximum.

Download date: 20-04-2024

Chapter 2

Background Information on Indentation

Abstract

This chapter provides some background information about indentation. It covers several commonly used hardness definitions in practice. It also provides some brief information about Hertz's theory of spherical and cylindrical indentation. A review about contact area determination technique used in nano indentation experiments is also included. Last section shows a phenomenon known as "indentation size effect" in several indentation experiments.

2.1 Indentation hardness

Hardness is an important property of a material. In general common sense, hardness is a measure of a material's resistance to deformation. However, the term hardness can also refer to material's resistance to compression, stretching, cutting and bending. In this thesis, hardness is used in the more technical sense of the material's resistance to indentation, and formally it is defined as the indentation force divided by contact area.

In practice, usually in engineering, indentation is performed by indenters of various shapes, each leading to its definition of hardness. The following subsections summarise the best known types of hardness.

2.1.1 Brinell hardness test

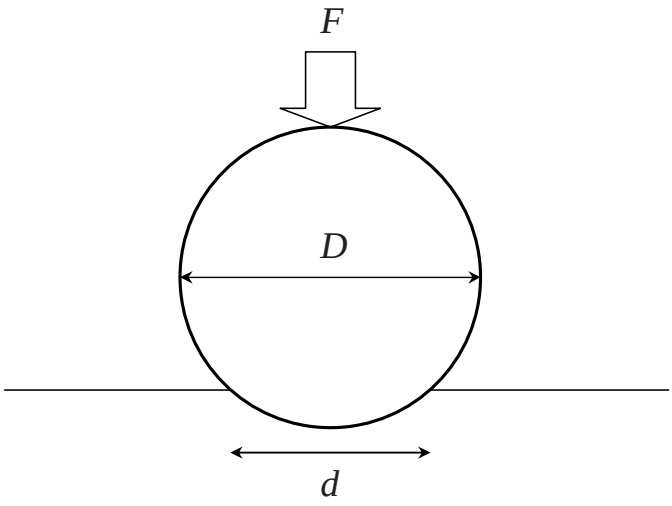

Figure 2.1 Brinell indentation testing schematic

The Brinell hardness refers to the hardness measured by indentation with a spherical indenter. Typically $D = 10$ mm diameter spheres are applied using 30 kN force for a duration of around 30 seconds. For softer materials the force can be reduced to 15 kN or even 5 kN. The diameter of the impression, d, left in the test material after the indenter is removed is measured with a microscope. The Brinell hardness number is calculated by dividing the force F applied by the surface area of the spherical cap left after indentation

$$H_{\mathrm{B}} = \frac{F}{D\left(D - \sqrt{D^2 - d^2}\right)\pi/2}, \tag{2.1}$$

where D and d are the diameters of the indenter and the impression, respectively (see Fig. 2.1). The Brinell indentation test was first proposed by Johan August Brinell, a Swedish engineer, in 1900, and was the first standardised hardness test in engineering.

2.1.2 Vickers hardness test

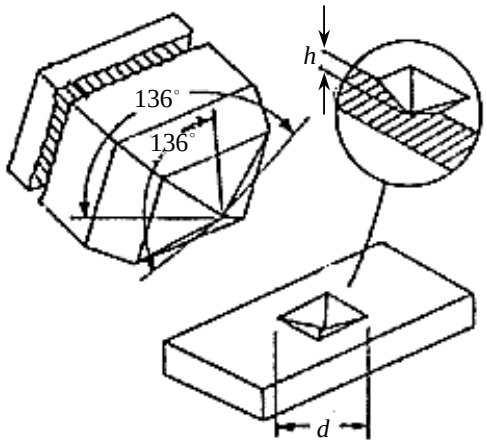

Figure 2.2 Vickers indenter schematic. The angles between opposite faces are both 136°. The diagonal of the impression area is d. The zoomed inset is the cross-section of the impression area having an indentation depth h.

The Vickers hardness is measured by indenting the test material with a diamond pyramidal-shape indenter. The indenter has the form of a right pyramid with a square base and an angle of 136° between opposite faces (Fig. 2.2). The indentation is subjected to a force ranging from 10 to 1000 N for duration around 10 to 15 seconds. The two diagonals of the impression area left in the surface of the material after the indenter is removed are measured using a microscope and their average d is calculated. If $A = \frac{1}{2}d^2/\sin(136°/2)$ is the area of the sloping surface of the impression, and F is the indentation force, then the Vickers hardness F/A, or

$$H_{\mathrm{V}} = \frac{F}{\frac{1}{2}d^2/\sin(136°/2)} \approx 1.854\frac{F}{d^2}. \tag{2.2}$$

The Vickers hardness test was firstly developed in the early 1920s.

2.1.3 Rockwell hardness test

The Rockwell hardness scale characterises the indentation hardness of materials through the depth of penetration of a cone or spherical indenter, loaded on a mate-

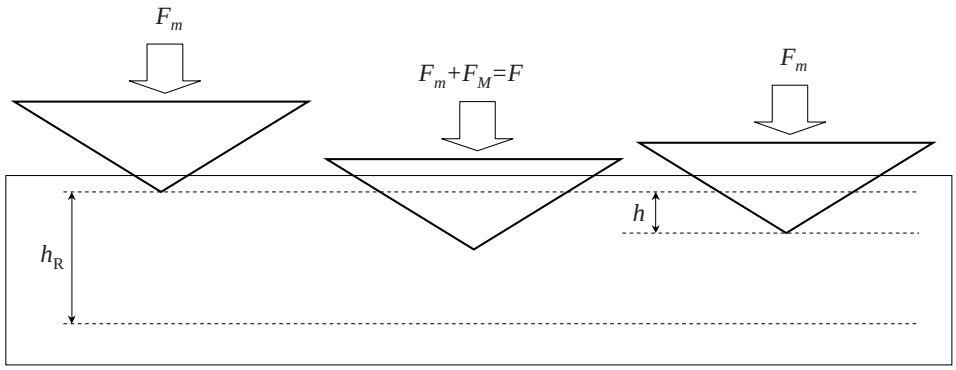

Figure 2.3 Rockwell indentation testing schematic, from left to right: initial minor loading (here the depth is defined as a reference depth), minor+major loading and minor loading only after major loading is removed.

rial sample and compared to the penetration in some reference material. It involves the use of a minor loading F_m followed by a major loading F_M, and finally the release the major loading as illustrated in Fig. 2.3. The hardness value directly according to:

$$H_\mathrm{R} = h_\mathrm{R} - h, \tag{2.3}$$

where h_R is the reference depth and h is the depth when F_M is removed. Both h_R and h are measured relative to the initial depth when the indentation was only loaded by F_m (see Fig. 2.3). Both h_R and h are measured in units of 0.002 mm. H_R is expressed in scale (HRA, HRB, ... , HRV), see Table. 2.1, depending on the indenter shape and applied major load. As an example, very hard steel for knife has Rockwell hardness value between HRC 55 to HRC 62.

Rockwell hardness testing is very common in the United States. Its popularity in commercial enterprises arises from its speed, robustness, resolution and small area of indentation.

2.1.4 Knoop hardness test

Knoop indentation testing is mainly used to measure hardness at the micro scale. The Knoop indenter is a diamond ground to the pyramidal form, as shown in Fig. 2.4, that produces a diamond shaped indentation which have a ratio between long and short diagonals of approximately 7:1. When Knoop hardness is measured, only the longest diagonal L of the indentation is measured. The shortest diagonal is calculated as $w = L\tan(130°/2)/\tan(172.5°/2)$, thus the impression area is $A = \frac{1}{2}wL = \frac{1}{2}L^2\tan(130°/2)/\tan(172.5°/2)$. Finally the knoop hardness is calculated

Scale	Indenter	F_{m} (N)	F_{M} (N)	h_{R}
HRA	conical diamond	100	500	100
HRB	$\frac{1}{16}$" spherical steel	100	900	130
HRC	conical diamond	100	1400	100
HRD	conical diamond	100	900	100
HRE	$\frac{1}{8}$" spherical steel	100	900	130
HRF	$\frac{1}{16}$" spherical steel	100	500	130
HRG	$\frac{1}{16}$" spherical steel	100	1400	130
HRH	$\frac{1}{8}$" spherical steel	100	500	130
HRK	$\frac{1}{8}$" spherical steel	100	1400	130
HRL	$\frac{1}{4}$" spherical steel	100	500	130
HRM	$\frac{1}{4}$" spherical steel	100	900	130
HRP	$\frac{1}{4}$" spherical steel	100	1400	130
HRR	$\frac{1}{2}$" spherical steel	100	500	130
HRS	$\frac{1}{2}$" spherical steel	100	900	130
HRV	$\frac{1}{2}$" spherical steel	100	1400	130

Table 2.1 Rockwell hardness scales. The spherical steel diameter is measured in inches ("). h_{R} is, traditionally, measured in units of 0.002 mm.

using

$$H_{\mathrm{K}} = \frac{F}{A} = \frac{F}{CL^2}, \tag{2.4}$$

where $C = \frac{1}{2}\tan(130°/2)/\tan(172.5°/2) \approx 0.07028$.

2.1.5 Berkovich hardness test

Berkovich indenter is commonly used for nano- and micro-indentation. It has three sided pyramid shape with the face angle 65.3° (see Fig. 2.5). The hardness is calculated as F/A_{c}, where F and A_{c} are the indentation force and projected contact area of the impression, respectively. By geometry, the contact area projection is calculated as $A_{\mathrm{c}} = 3\sqrt{3}\tan^2(65.3°)h_{\mathrm{c}}^2 \approx 24.56h_{\mathrm{c}}^2$. The contact area measurement is discussed further in Section 2.3.

2.1.6 Relation between hardness and yield stress

During early indentation, the material deforms elastically, and when indentation advances, the deformation turns to be plastic. Sequentially, there are three ranges

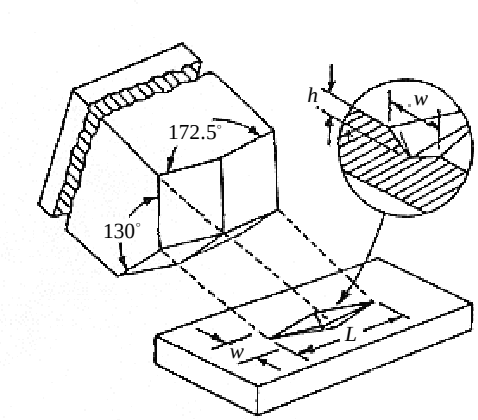

Figure 2.4 Knoop indenter schematic. The angles between opposite faces are 172.5° and 130°. The long and short diagonals of the impression area are L and w, respectively. The zoomed inset is the cross-section of the impression area having an indentation depth h.

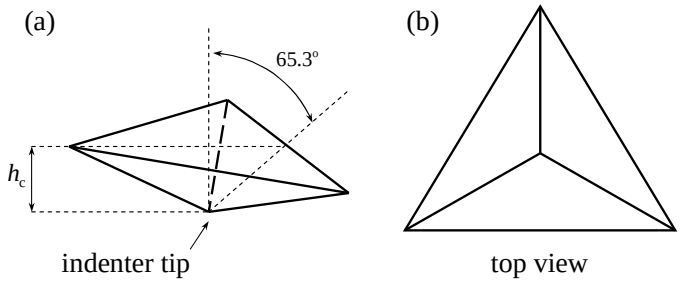

Figure 2.5 Berkovich indenter schematic. (a) Indenter impression tip with the face angle is 65.3°. The contact depth is h_c. (b) Top view of the impression area.

of deformation during indentation: pure elastic, elastic-plastic and pure plastic. On the transition between pure elastic region and elastic-plastic region, the material starts to yield plastically, *i.e.* irreversible deformation starts to emerge. Similar phenomenon happens in tensile (or compression) test, where the stress state during the transition between elastic and plastic deformation is commonly known as "yield stress". Usually the yield stress is defined as the stress at an offset strain is 0.2% (Fig. 2.6.

Tabor related the indentation hardness H to the yield stress σ_Y [1, 2, 3] as

$$H = C\sigma_Y, \tag{2.5}$$

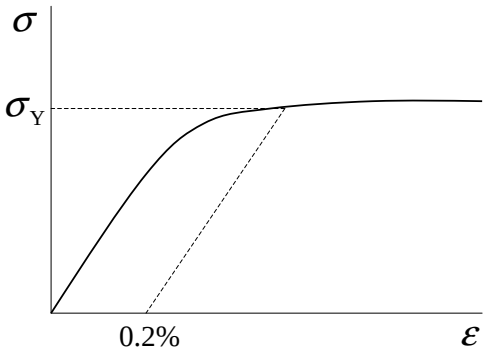

Figure 2.6 Schematic of a tensile (or compression) test. The yield stress usually is taken at 0.2% plastic strain.

where for self-similar, such as conical or pyramidal, indenters the value of the constant C is close to 3, provided that the work hardening is neglected. The exact value slightly depends on the indenter geometry. For indenters with $\alpha > 60°$, where 2α is the tip sharpness angle, the value of C ranges from 2.5 to 3 [3]. This simple relation is useful in practical engineering to extract the yield stress from an indentation test.

2.2 The mechanics of contact: Hertz's theory

Indentation is nothing more than a special case of bringing two bodies into contact, in which one of them –the indenter– is relatively stiff, and the other is the specimen whose properties are to be measured. To understand what is measured during indentation, we have to begin with a brief summary of classical theories about the contact between an indenter and large flat sample of material.

In 1882, Hertz analysed the stress at the contact of two elastic solid bodies [4] motivated by his study about Newton's optical interference fringes in the gap between two glass lenses. He was concerned about the influence of elastic deformation of the lens surfaces during contact due to the pressure between them. He started to investigate elasticity in order to understand the reversible change in the lens surface change.

In his theory, Hertz made the following assumptions:
(i) The surfaces are continuous and non-conforming;
(ii) The strains are small;
(iii) Each body can be considered as an elastic half-space;
(iv) The contact is frictionless.

2.2.1 Spherical indentation

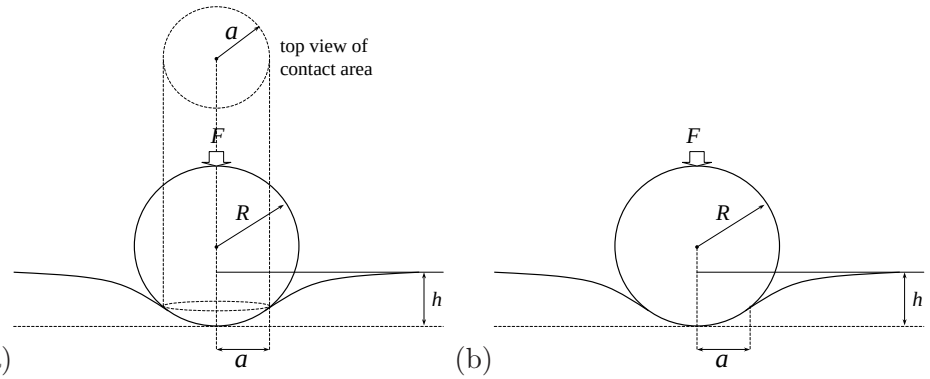

Figure 2.7 Schematics of (a) spherical and (b) cylindrical indentation. R is indenter radius, h is indentation depth, F is indentation force, and a is contact radius and half contact length for spherical and cylindrical indenter, respectively.

For spherical contact between isotropic materials, the contact area will be circular and Hertz showed that the radius a of the contact area is given by [4]

$$a^3 = \frac{3}{4}\frac{FR}{E^*}, \tag{2.6}$$

where F and R are the applied force and combined radius of curvature curvature, respectively. The reduced modulus E^* is defined as

$$\frac{1}{E^*} = \frac{1-\nu_1^2}{E_1} + \frac{1-\nu_2^2}{E_2}, \tag{2.7}$$

where E's and ν's are Young's moduli and Poisson's ratio, respectively, and indices 1 and 2 refer to the first and the second body, respectively. It is defined in general case where the indenter is not rigid, and the reduced modulus E^* is defined in the same manner as two springs in series. The combined radius is defined by

$$\frac{1}{R} = \frac{1}{R_1} + \frac{1}{R_2}. \tag{2.8}$$

In the case of indentation by a rigid spherical indenter (Fig. 2.7a), the first body being the indenter and the second being the indented material, R reduces to the radius of the indenter and the reduced modulus $E^* = E/(1-\nu^2)$, where $E = E_2$ is the modulus of the material.

In seeing with the assumptions listed above, the Hertzian representation of contact is only local, and does not capture the overall bulk mechanics of the two contacting bodies.

In Hertz's solution, the vertical displacement of a point on the surface within the area of contact is given by

$$u_3(r) = \frac{3F}{8aE^*}\left(2 - \frac{r^2}{a^2}\right), \tag{2.9}$$

where $r \leq a$, and r is the radial distance from the symmetry axis. The contact pressure distribution reads

$$p(r) = p_0\left(1 - \frac{r^2}{a^2}\right)^{1/2}, \tag{2.10}$$

where p_0 is the maximum pressure, *i.e.* pressure at the axis of symmetry. It is related to the applied force through

$$F = \int_0^a p(r) 2\pi r \, \mathrm{d}r = \frac{2}{3} p_0 \pi a^2, \tag{2.11}$$

or

$$p_0 = \frac{3F}{2\pi a^2}. \tag{2.12}$$

The depth of indentation is

$$h = u_3(0) = \left(\frac{9F^2}{16RE^{*2}}\right)^{1/3} = \frac{a^2}{R}. \tag{2.13}$$

It is convenient to express the maximum pressure p_0 independent from the contact radius a, by eliminating it through Eq. (2.6) to get

$$p_0 = \left(\frac{6FE^{*2}}{\pi^3 R^2}\right)^{1/3}. \tag{2.14}$$

2.2.2 Cylindrical indentation

For contact of infinitely-long cylindrical bodies, with both axes lying parallel to the x_3 direction, the system is pressed in contact with a force F per unit length, the problem becomes a two-dimensional one. The relative radius R and reduced modulus E^* are defined in the same manner as for spherical contact, see Eqs. (2.7) and (2.8). Again, for the case of rigid cylindrical indentation (Fig. 2.7b), one of the bodies, say, the second body, becomes the indenter and has radius $R = R_2$ and reduced modulus $E^* = E_2/(1 - \nu^2)$.

Hertz derived the expression for the pressure distribution on the surface [4] as

$$p(x_1) = \frac{2F}{\pi a^2}(a^2 - x_1^2)^{1/2}, \tag{2.15}$$

where a is the half contact are per unit length, given by

$$a^2 = \frac{4FR}{\pi E^*} \tag{2.16}$$

and the maximum pressure is

$$p_0 = \sqrt{\frac{FE^*}{\pi R}}. \tag{2.17}$$

McEwen [4, 5] expressed the stresses at a general point (x_1, x_2) as

$$\sigma_{11} = -\frac{p_0}{a}\left[m\left(1+\frac{x_2^2+n^2}{m^2+n^2}\right)-2x_2\right], \tag{2.18a}$$

$$\sigma_{22} = -\frac{p_0}{a}m\left[1-\frac{x_2^2+n^2}{m^2+n^2}\right], \tag{2.18b}$$

$$\sigma_{12} = \frac{p_0}{a}n\left[\frac{m^2-x_2^2}{m^2+n^2}\right], \tag{2.18c}$$

where

$$m^2 = \frac{1}{2}\left[\sqrt{(a^2-x_1^2+x_2^2)^2+4x_1^2x_2^2}+(a^2-x_1^2+x_2^2)\right], \tag{2.19a}$$

$$n^2 = \frac{1}{2}\left[\sqrt{(a^2-x_1^2+x_2^2)^2+4x_1^2x_2^2}-(a^2-x_1^2+x_2^2)\right]. \tag{2.19b}$$

The maximum shear stress at any point

$$\tau_{\max} = \sqrt{\sigma_{12}^2+\frac{1}{4}(\sigma_{22}-\sigma_{11})^2}, \tag{2.20}$$

has a peak of $\tau_{\max} = 0.3p_0$ at $(0, 78a)$.

2.3 Contact stiffness method for contact area determination in nano-indentation

Nano-indentation is commonly used to probe the material hardness at small scales. A typical schematic of a nano-indenter device is shown in Fig. 2.8. Figure 2.9 shows an example of an indenter tip photograph. Since hardness is defined as indentation force divided by contact area, it is important to measure the contact area accurately. However, it is difficult to measure the actual contact area due to sink-in effects and roughness of the surface.

Oliver and Pharr have developed a technique for determining contact area [6, 7]. The method begins by analysing the force versus depth curve of indentation data, including the unloading branch, as illustrated in Fig. 2.10. From force-depth curve,

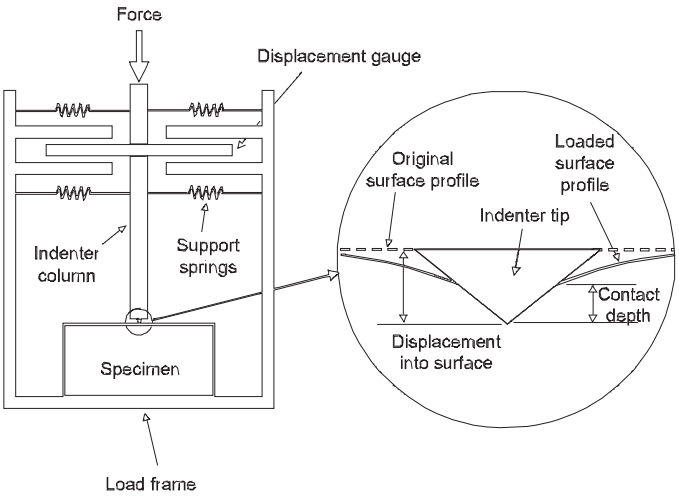

Figure 2.8 Schematic of nano-indenter device.

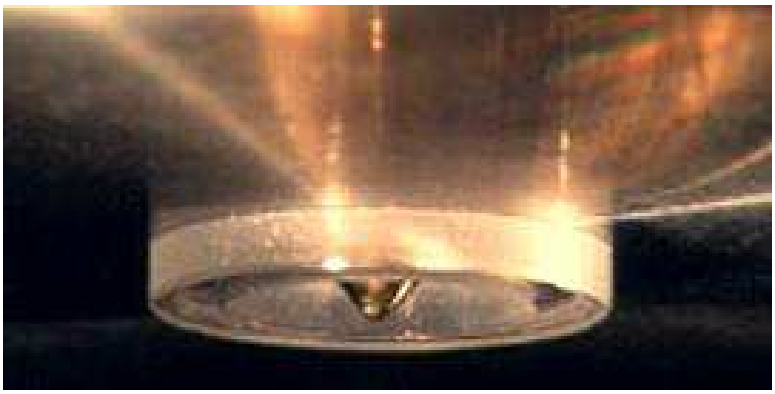

Figure 2.9 Photograph of a conical indenter with a blunt tip.

one can measure peak force $F_{\max}$, depth at peak force $h_{\max}$ and final depth h_{f}, *i.e.* the depth after withdrawal of the indenter. Sneddon's expression for the stiffness S at initial unloading [8]

$$S = \left.\frac{\mathrm{d}F}{\mathrm{d}h}\right|_{F=F_{\max}} = \frac{2}{\sqrt{\pi}} E^* \sqrt{A_{\mathrm{c}}} \tag{2.21}$$

relates the contact area A_{c} to the reduced modulus E^*. This expression assumes that the initial portion of unloading curve is elastic. Pharr *et al.* have shown that

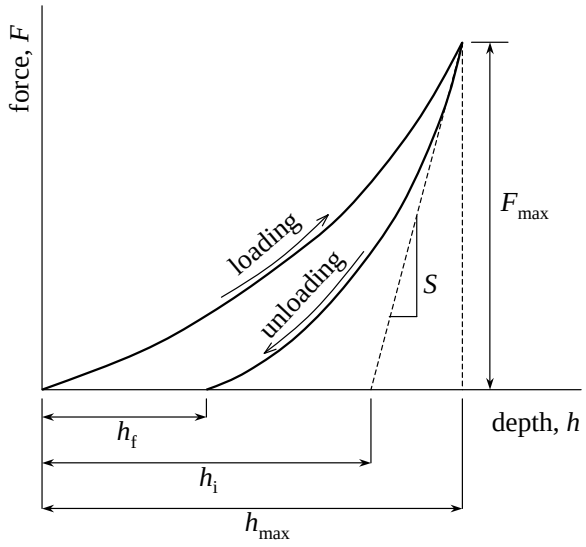

Figure 2.10 Schematic representation of force versus depth for an indentation experiment. Stiffness S is determined from initial unloading curve. $F_{\max}$ and $h_{\max}$ is the peak force and its corresponding depth, respectively. h_{f} is the final depth after removal of the indenter. h_{i} is the intercept depth by, *i.e.* linear extrapolation of the initial unloading curve to $F = 0$.

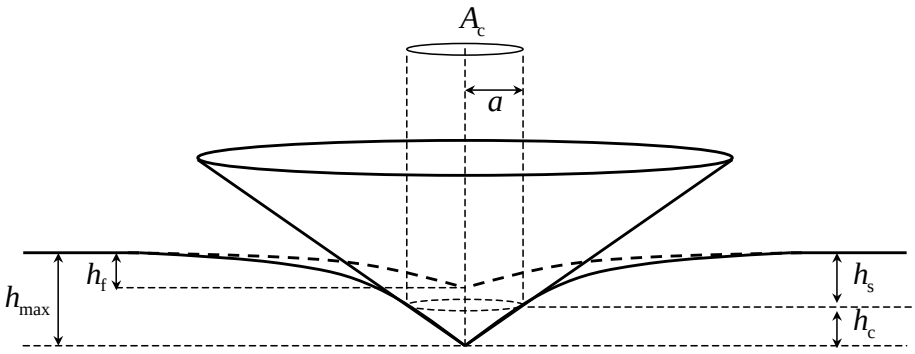

Figure 2.11 Geometry to characterise indentation: A_{c} and a are the projected contact area and its radius, respectively, h_{c} is the sink-in depth.

Eq. (2.21) applies to any indenter with an axisymmetric geometry [9], and even works rather well (with only small deviation) for at least some non-axisymmetric indenters [10]. Experimentally measuring S, however, is not trivial since one has

to decide how much of the initial unloading portion should be taken to determine S accurately. Oliver and Pharr proposed to fit the initial unloading curve by the power law

$$F = A_0(h - h_\mathrm{f})^m, \tag{2.22}$$

and to use this relation in the definition $S = \mathrm{d}F/\mathrm{d}h$, *i.e.*

$$S|_{F=F_\mathrm{max}} = mA_0(h_\mathrm{max} - h_\mathrm{f})^{m-1}. \tag{2.23}$$

In these expressions, A_0 is a constant depending on geometry, material and indenter moduli and Poisson's ratios, and m depends on the tip geometry. Table 2.2 shows typical values of m for several indenter geometries:

Indenter geometry	m	η
Flat ended cylindrical punch	1.0	1.0
Paraboloid of revolution	1.5	0.75
Cone	2.0	0.72

Table 2.2 Typical values of m and η for several indenter geometries.

The determination of the contact area A_c proceeds by estimating the contact depth $h_\mathrm{c} = h_\mathrm{max} - h_\mathrm{s}$, as defined in Fig. 2.11, and using the tip geometry to compute A_c from this. Sneddon's analysis for the elastic displacement outside the contact perimeter gives the relation for the sink-in depth h_s [8]:

$$h_\mathrm{s} = \eta\frac{F_\mathrm{max}}{S}, \tag{2.24}$$

where η is a constant that depends on the shape of the indenter (see Tab. 2.2. Since $F_\mathrm{max}/S = h_\mathrm{max} - h_\mathrm{i}$, Eq. (2.24) can be rewritten as

$$h_\mathrm{c} = h_\mathrm{max} - \eta(h_\mathrm{max} - h_\mathrm{i}), \tag{2.25}$$

where h_i is the intercept depth, *i.e.* the interception of linear extrapolated initial unloading slope to $F = 0$.

To calculate contact area A_c and reduced modulus E^*, Oliver and Pharr proposed an iterative procedure as follows [6]:
[Step 1] Model the load frame of the indenter and the specimen as two springs in series with a total compliance

$$C = C_\mathrm{s} + C_\mathrm{f}, \tag{2.26}$$

where $C = 1/S$ is the total measured compliance, $C_\mathrm{s} = 1/S_\mathrm{s}$ is the specimen's compliance and $C_\mathrm{f} = 1/S_\mathrm{f}$ is the load frame's compliance. Eq. (2.26) together with

Eq. (2.21) can be written as

$$C = C_{\mathrm{f}} + \frac{\sqrt{\pi}}{2E^*} A_{\mathrm{c}}^{-1/2}. \tag{2.27}$$

[Step 2] Determine C and initial estimate value of A_{c} for several loading-unloading cycles with various indent size, *i.e.* to get a set of (C, A_{c}) data pairs. The initial estimate of A_{c} can be given by $A_{\mathrm{c}} = 24.56 h_{\mathrm{c}}^2$ for Berkovich indenter or $A_{\mathrm{c}} = \pi(h_{\mathrm{c}} \tan\alpha)^2$ for conical indenter, where α is half of the conic angle.
[Step 3] Plot C versus $A_{\mathrm{c}}^{-1/2}$ and fit a straight line according to Eq. (2.27) to get estimate values of C_{f} and E^*.
[Step 4] Use C_{f} and E^* obtained, calculate the contact areas A_{c} by rewriting Eq. (2.27) as

$$A_{\mathrm{c}} = \frac{\pi}{4(E^*)^2 (C - C_{\mathrm{f}})^2}, \tag{2.28}$$

to get a set of (A_{c}, h_{c}) data pairs.
[Step 5] Use (A_{c}, h_{c}) data pairs from step 4, fit A_{c} versus h_{c} to the polynomial

$$A_{\mathrm{c}} = C_0 h_{\mathrm{c}}^2 + C_1 h_{\mathrm{c}} + C_2 h_{\mathrm{c}}^{1/2} + C_3 h_{\mathrm{c}}^{1/4} + \cdots + C_8 h_{\mathrm{c}}^{1/128}, \tag{2.29}$$

where $C_0 = 24.56$ for Berkovich or $C_0 = \pi \tan^2\alpha$ for conical indenter. C_1 through C_8 are the fitting parameters to be determined; they describe a deviation from indenter sharpness due to blunting at the tip.
[Step 6] With the new value of A_{c}, go back to step 3 until the convergence is achieved.

2.4 Experimental indentation size effects of hardness

The phenomenon where hardness decreases with increasing indentation size –known as the "indentation size effect"– has been observed in many indentation experiments. The size effect relates to how we define "size", as will be discussed in detail in chapter 4). Here we briefly summarise several results of indentation experiments, in which size effects are reported.

Mirsham and Parakala [11] have found this effect in nickel single crystals using Berkovich, cube corner and conical indenters. As an example, Fig. 2.12 shows hardness versus depth in nickel using a conical indenter. The hardness is decreasing with increasing depth, except for very shallow depths where the hardness increases due to the blunt tip of the indenter.

Swadener *et al.* have observed an indentation size effect as a function of indenter radius R in annealed iridium measured with spherical indenter [12], as shown in Fig. 2.13. When measuring the hardness at a constant value of the contact to indenter radius ratio of $a/R = 0.05$, the hardness decreases with increasing tip radius.

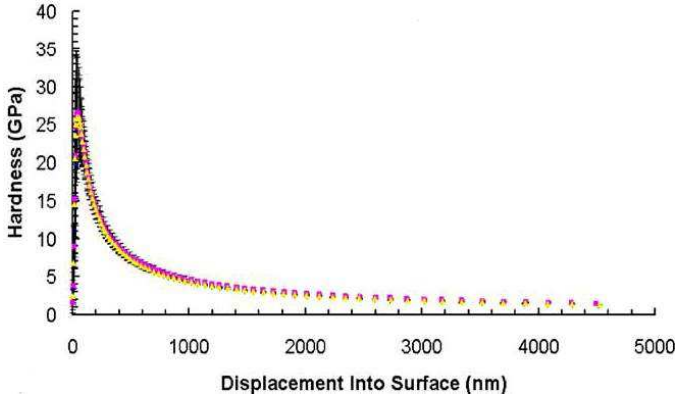

Figure 2.12 Indentation size effect in hardness from indentation of nickel using conical indenter (at various strain rates, indicated by the different colours), as observed by Mirshams and Parakala [11]. This figure is reprinted from [11] with permission from Elsevier.

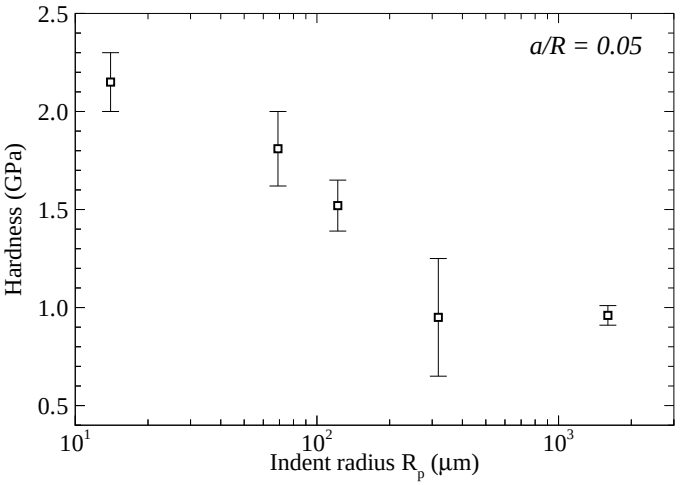

Figure 2.13 Indentation size effect of hardness in annealed iridium measured with spherical indenters with different radii R at constant ratio $a/R = 0.05$. This figure is reproduced from [12].

While the above-referenced results were for single crystals, Manika and Maniks [13] have also reported indentation size effects in various amorphous solids, as shown in Fig. 2.14a. In polycrystalline copper, they found size effects similar to those in single crystals as long as the grain size was larger than 5 μm, see Fig. 2.14b.

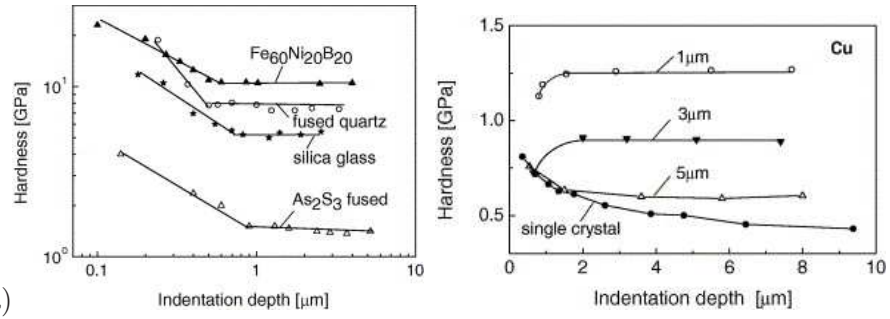

Figure 2.14 Indentation size effects observed by Manika and Maniks [13] in (a) various amorphous solids and (b) polycrystal copper for various grain size. This figure is reprinted from [13] with permission from Elsevier.

References

[1] D. Tabor, The hardness and strength of metals. *Journal of the Institute of Metals*, 79:1–18, 1951.

[2] K.L. Johnson, The correlation of indentation experiments. *Journal of the Mechanics and Physics of Solids*, 18:115–126, 1970.

[3] R. Hill, *The Mathematical Theory of Plasticity*. Oxford University Press Inc., New York, USA, 1950.

[4] K.L. Johnson, *Contact Mechanics*, Cambridge: Cambridge University Press, 1985.

[5] E. McEwen, Stresses in elastic cylinders in contact along a generatrix. *Philosophical Magazine*, 40:454, 1949.

[6] W.C. Oliver and G.M. Pharr, An improved technique for determining hardness and elastic-modulus using load and displacement sensing indentation experiments. *Journal of Materials Research*, 7:1564–1583, 1992.

[7] W.C. Oliver and G.M. Pharr, Measurement of hardness and elastic modulus by instrumented indentation: Advances in understanding and refinements to methodology. *Journal of Materials Research*, 19:3–20, 2004.

[8] I.N. Sneddon, The relation between load and penetration in the axisymmetric Boussinesq problem for a punch of arbitrary profile. *International Journal of Engineering and Science*, 3:47–57, 1965.

[9] G.M. Pharr, W.C. Oliver and F.R. Brotzen, On the generality of the relationship between contact stiffness, contact area, and elastic modulus during indentation. *Journal of Materials Research*, 7:613, 1992.

[10] R.B. King, Elastic analysis of some punch problems for a layered medium. *International Journal of Solids and Structures*, 23:1657–1664, 1987.

[11] R.A. Mirshams and P. Parakala, Nanoindentation of nanocrystalline Ni with geometrically different indenters. *Materials Science and Engineering A*, 372: 252-260, 2004.

[12] J.G. Swadener, E.P. George, and G.M. Pharr, The correlation of the indentation size effect measured with indenters of various shapes. *Journal of the Mechanics and Physics of Solids*, 50:681–694, 2002.

[13] I. Manika and J. Maniks, Size effects in micro- and nanoscale indentation. *Acta Materialia*, 54:2049–2056, 2006.